Progress on the Development of the Radio-Frequency Quantum Upconverter

Jason Corbin[a,*]
[a]Stanford University, Department of Physics, Stanford, California, United States, 94305

*Jason Corbin, jycorbin@stanford.edu

1 Introduction

Many Circuit Quantum Electrodynamics (cQED) techniques exist for manipulating and engineering quantum states of microwave photons above 1 GHz.[1] The development of these techniques have led to increasingly sensitive probes of fundamental physics. Unlike microwave frequencies, quantum electromagnetic measurements below 300 MHz (which we will broadly refer to as "MHz signals") have not been well developed. This is because at these frequencies and dilution refrigerator temperatures, MHz resonators exist in thermal states (with $k_B T/h\nu \gtrsim 1$ with $T \approx 10$ mK), which means that common cQED techniques like photon counting do not significantly enhance the sensitivity of the experiment.

There is a growing interest in developing quantum protocols for this range of frequencies. In particular, searches for the sub-μeV axion aim to detect electromagnetic signals over a wide range of frequencies (100 Hz to 300 MHz).[2–7] Although resonant circuits at these frequencies are thermal, they can carry useful information detuned from the resonant frequency where thermal noise rolls off.[8,9] Applying quantum protocols like backaction evasion to signals at these frequencies can significantly increase the effective bandwidth of a resonator while maintaining constant signal-to-noise ratio, meaning that an axion search can scan over frequency space significantly faster.

The Radio-Frequency Quantum Upconverter (RQU) is a superconducting device that couples MHz signals in our range of interest with GHz frequency carrier waves. By using a flux-tunable interferometer to modulate the resonance frequency of a GHz quarter-wave resonator, a MHz signal can be upconverted to a GHz sideband of the carrier wave. This upconversion allows for our MHz signals to interface with the mature cQED technology in the GHz range. In addition, as a superconducting quantum device that couples GHz and MHz signals, the RQU provides a natural method of implementing quantum protocols at like backaction evasion.

This report will discuss progress that has been made in the last year with RQUs. Section 2 will include a description of the design of our current generation of RQUs, as well as provide any necessary background for discussing results. Section 3 will describe RQU fabrication and improvements made to this process in the past year. Section 4 will cover results taken with recently fabricated RQUs, including a demonstration of upconversion, frequency shifts from flux modulation, and phase-sensitive amplification. Section 5 will discuss next steps in RQU research, covering in particular what our goals are for the next year.

2 RQU Design

A circuit diagram representation of the RQU can be seen in figure 1 on the left. The RQU consists of a GHz resonator with a flux-tunable inductance, which is coupled to a pick up coil that detects MHz electromagnetic signals. This is capacitively coupled to a feedline with a microwave drive. If the microwave drive is applied at the resonance frequency of the GHz resonator, the readout amplifier will see upconverted MHz signal data as sidebands detuned from the microwave drive frequency by the MHz frequency.

Our current design of RQUs can be seen on the right in figure 1. The flux-tunable inductor is a three Josephson junction interferometer, designed to decouple the GHz carrier wave from box modes in the MHz resonator. The GHz resonator is a length of 50 Ω coplanar waveguide which is

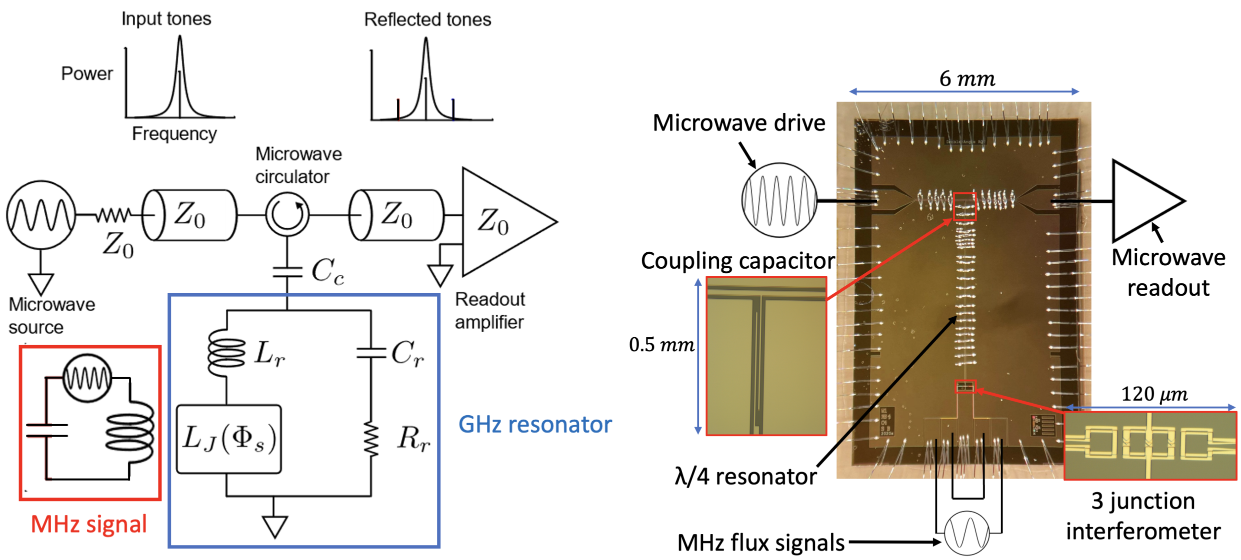

Fig 1: A fabricated RQU (right) with an equivalent circuit diagram of the RQU (left). The RQU consists of a MHz "pickup" resonator that couples to a GHz resonator through a flux-tunable inductance $L_J(\Phi_s)$. The GHz resonator is capacitively coupled through C_c to a transmission line, where a carrier tone at the GHz resonance frequency is expected to pick up sidebands detuned from the carrier frequency by the MHz signal. The actual RQU design uses a quarter-wave resonator with a three junction interferometer as the flux-tunable inductance. MHz signals are coupled into the quarter-wave resonator via "input coils" on either side of the interferometer.

designed to operate at around 5.5 GHz. Currently, our MHz pickup coil is replaced by a function generator operating at MHz frequencies. MHz flux is coupled into the GHz resonator via "input coils" that exist on either side of the three junction interferometer.

An in-depth quantum mechanical treatment of the RQU can be found in a paper published by our lab in the last year (Kuenstner et.al., 2022).[10] This includes the treatment of the RQU in analogy with cavity optomechanics and the use of input-output theory to describe the RQU. For this report, we will focus on describing background and motivation for the results we've obtained. We implore the reader to read through Kuenstner et.al. (2022) for a more complete understanding of the theory and operation of an RQU.

The purpose of an RQU is to implement quantum protocols like backaction evasion to increase the bandwidth of MHz electromagnetic signal searches. Without any quantum protocols, the best one can hope for with any sensor will be operating at the Standard Quantum Limit (SQL), which corresponds to a half photon of noise in each quadrature of our MHz signal. This noise limits our bandwidth - we can only maintain constant signal-to-noise ratio insofar as we are dominated by thermal noise (which has the same Lorentzian lineshape in frequency space as the MHz resonator response).

RQUs are designed to implement backaction evasion to evade the SQL. All backaction noise is shuffled into one quadrature of our MHz signal and the other quadrature is read out. To implement this, one would need to drive the MHz resonator in one quadrature only and effectively leave the other quadrature of noise ”unmeasured.” A demonstration of this would amount to a measurement of “phase-sensitive amplification,” in which the upconverted MHz signal amplitude decreases dramatically if the MHz drive is 90^o out of phase with the MHz flux signal. A demonstration of phase-sensitive amplification, in addition to a demonstration of upconversion, will be presented in Section 4.

3 Progress on Fabrication

Current generations of RQUs are fabricated using shadow evaporation. A description of this technique is described in figure 2. Briefly, shadow evaporation involves creating a stack of photoresists with an overhanging layer of resist. Metal is deposited at two different angles so that a “shadow” of the resist pattern is deposited with some offset. Some areas of the design will contain a photoresist bridge - the angled deposition then serves to deposit metal underneath this bridge such that the design overlaps itself on either side. By including an oxidation step in between metal depositions, the overlapping layer of metal created underneath these bridges forms the Josephson junctions of our devices.

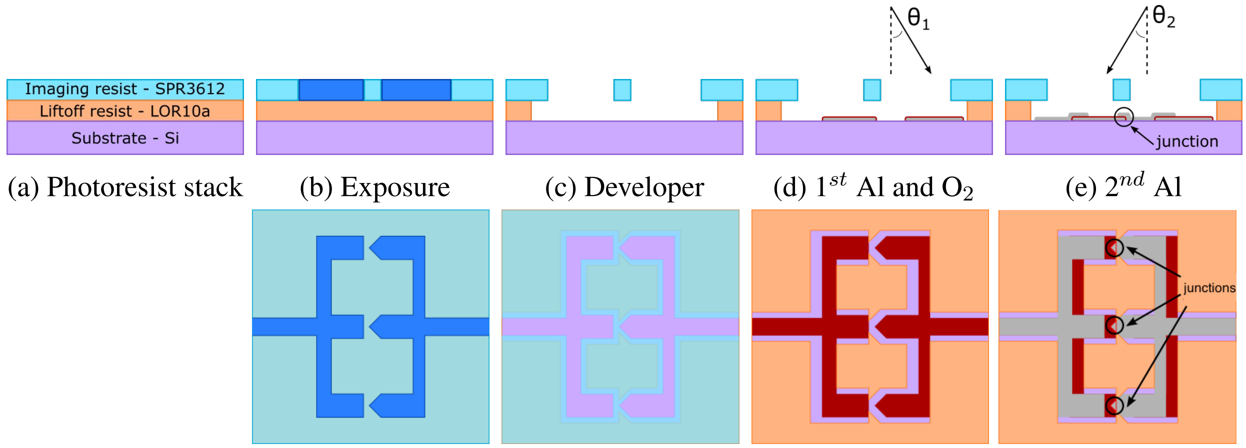

Fig 2: A diagram representing the steps of shadow evaporation. The top images are viewing a slice of the wafer from the side, the bottom images are viewing from above. (2a) A stack of liftoff resist (LOR10a) and imaging resist (SPR3612) are spun onto a silicon substrate. (2b) The stack of resists are exposed in the ASML PAS 5500/60 i-line stepper, patterning the resist with our RQU. (2c) Developer washes away any exposed imaging resist as well as an undercut layer of liftoff resist, leaving overhangs and bridges of imaging resist. (2d) Aluminum is deposited in the Plassys electron beam evaporator at a 32^o angle, leaving the first shadow of our device. Oxygen is flowed into the Plassys chamber at 50 torr for 10 minutes to create an AlO_x insulating layer. (2e) Aluminum is deposited at a 32^o angle in the other direction, leading to overlapping junctions underneath the imaging resist bridge. These form the triangular junctions of our three junction interferometer.

The lithography and liftoff processes are performed at the Stanford Nanofabrication Facility. Our RQU fabrication process uses a silicon substrate and a stack of imaging resist (Shipley 3612) and liftoff resist (LOR10a) with 1μm thickness, which we expose in an ASML PAS 5500/60 i-line stepper and develop. The extent of undercut is controlled by softbake temperature, bake time, and developer application time.

Our devices are fabricated with Al-AlO_x-Al junctions, and the deposition is performed using a Plassys electron beam evaporator. The angles of our deposition are controlled by tilting the wafer - for our most recently deposited and tested RQUs, the deposition angles (referencing figure 2) are $\theta_1 = 32^o$ and $\theta_2 = 32^o$. The first aluminum deposition step produces a 64 nm thick layer of aluminum, while the second aluminum deposition step produces a 100 nm layer of aluminum. The oxidation step between these aluminum depositions is performed by flowing oxygen into the

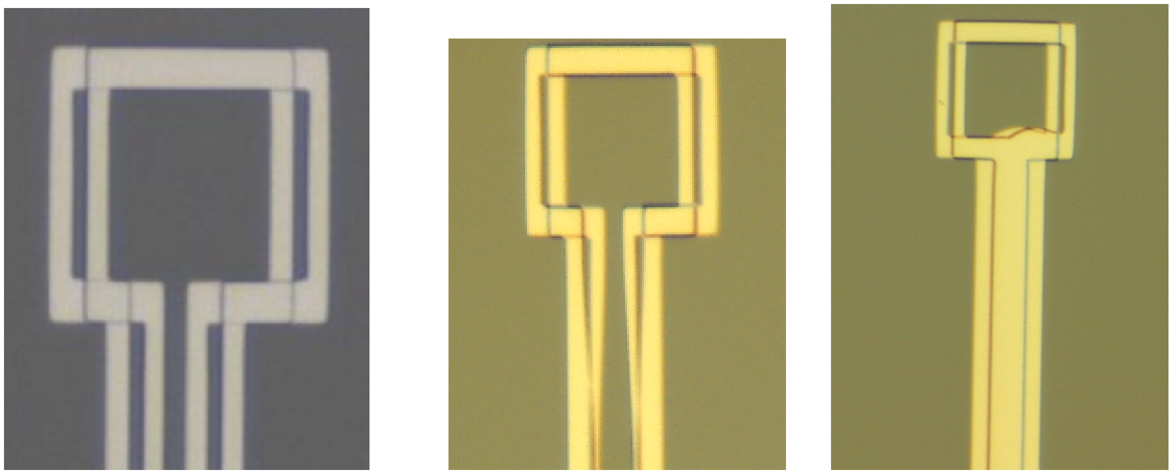

(a) (b) (c)

Fig 3: Example input coils exemplifying the types of errors produced due to improper softbaking of the liftoff resist. Figure 3a shows an example of a properly fabricated input coil. Figure 3b shows warping of the aluminum wires, while figure 3c shows the wires becoming completely merged together. Both errors in 3b and 3c are believed to be due to insufficient softbaking, leading to the underlying photoresist between the two wires to be completely undercut. 3b shows an example where the imaging resist collapses on the underlying silicon wafer and 3c shows an example of the undercut resist being torn off.

deposition chamber at 50 torr for 10 min (with ramp rate, final pressure, and exposure time advised by previous users that used the same system to create successful junctions).

After deposition, a liftoff step is performed to remove any resist and unwanted metal on the device. This process is designed to produce junctions with triangular overlapping regions, areas of overlap controlled by an "offset" parameters, and nominal critical current density of $1.26\mu A/\mu m^2$.

Over the past year, the fabrication process was improved and made more robust. In addition to the usual focus-exposure matrices used to fine-tune exposure, the undercut rate was optimized. Examples of the error modes experienced can be found in figure 3. These types of damage are believed to be due to insufficient softbaking. To troubleshoot this, several wafers were softbaked at a variety of different temperatures between 150C and 170C. In addition, the usual layer of foil between the hotplate and our wafer was removed to perform the softbake. The resulting photoresist images can be found in figure 4. Other than a circular defect from uneven hotplate temperatures

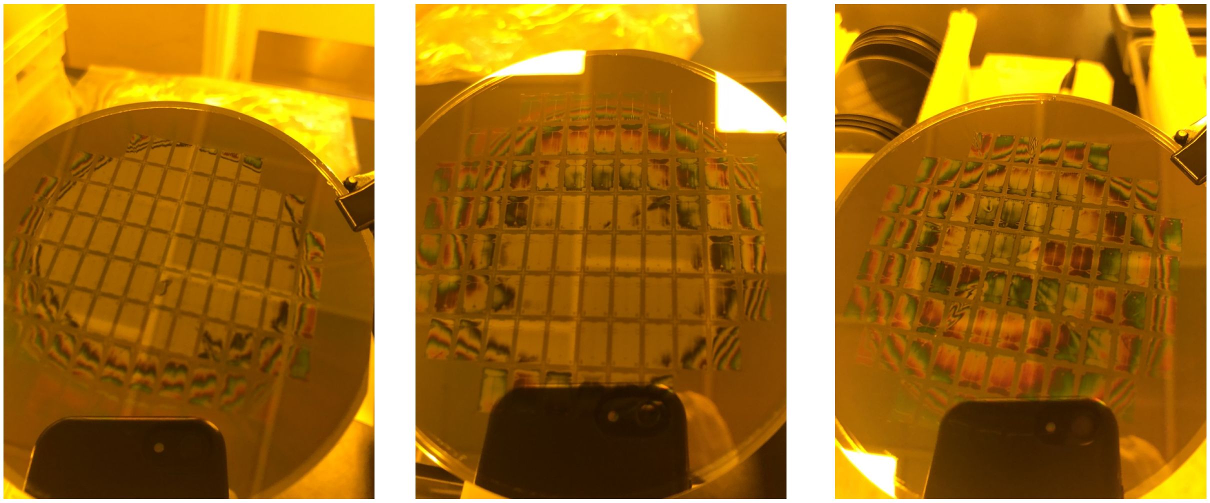

(a) (b) (c)

Fig 4: Some example wafers after different softbake temperatures. Each wafer was softbaked for 5 minutes, with Figure 4a baked at 150C, 4b baked at 160C, and 4c at 170C. The wafers become notably worse as temperature increases from 150C, with more resist residue remaining after our develop step as temperature increases. The devices towards the center of the 150C wafer contain no photoresist defects after examination under microscope. The circular pattern towards the edges of our device are suspected to be due to uneven heating of the hotplate.

(which should be solved by introducing a flat aluminum sheet instead of foil), our devices produced at the center of the 150C-baked wafer seem to be sufficient for the 1 μm features on our devices.

4 Results with Current RQUs

Several important measurements have now been reproduced on our current generation of RQUs, including the aforementioned demonstration of phase-sensitive amplification, flux-dependent frequency modulation, and upconversion. Our RQU is placed at the base stage of a ^{3}He sorption cryostat and operates at around 30 mK. Before the RQU, there are a variety of filters and attenuation, allowing for low-noise microwave tones to probe the RQU. After the RQU, there is a High Electron Mobility Transistor (HEMT) amplifier that provides low-noise amplification of the output of the RQU. The input coils, which provide flux to the interferometer on either side, is supplied with current via filtered and attenuated twisted pairs. A diagram of the set-up can be found in the

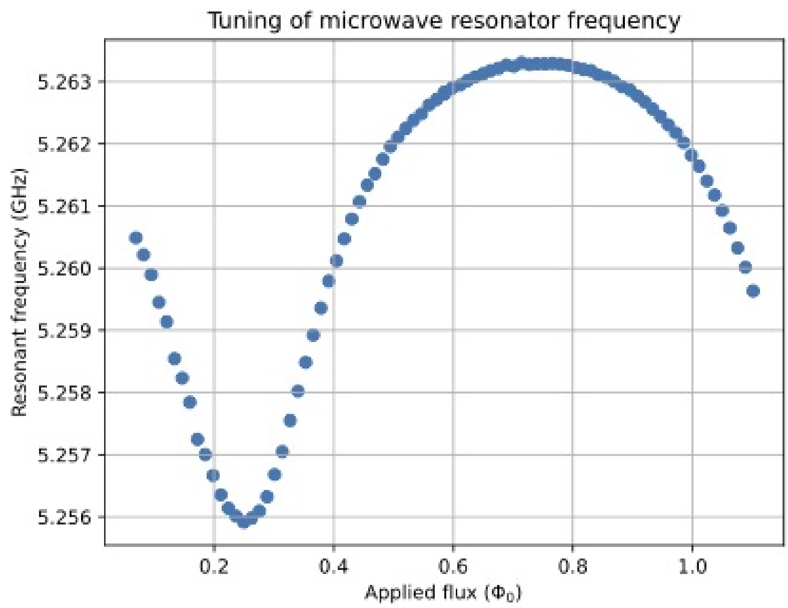

Fig 5: Demonstration of the frequency modulation of our RQU from applied flux to the interferometer. By sending current through the input coils of our device, we were able to modulate the resonance frequency of the GHz resonator by around 7 MHz.

paper Kuenstner et. al. (2022).[10]

Our device was initial probed with a Vector Network Analyzer. The device has a resonance frequency around 5.26 GHz. Applying DC currents between -4 to 4 mA to either coil to create a total applied flux, our RQU showed a 3.5 MHz flux-periodic swing in the resonance frequency of the GHz resonator. These results are shown in figure 5.

In addition, a spectrum analyzer was used to measure the response of our device to a microwave drive tone. Our first measurement was a demonstration of upconversion - for this, a probe tone set to 5.2591 GHz at 0 dBm was used, with 40 dB of attenuation outside the fridge and 20 dB of attenuation at each of 3 temperature stages before the RQU. The MHz signal was set to 1 V_{pp} with a 9 kOhm resistor leading into the twisted pair. As can be seen in figure 6, the results of inputting 500kHz, 2MHz and 8MHz flux inputs into the interferometer are the creation of sidebands on the carrier wave detuned by 500kHz, 2MHz, and 8MHz respectively.

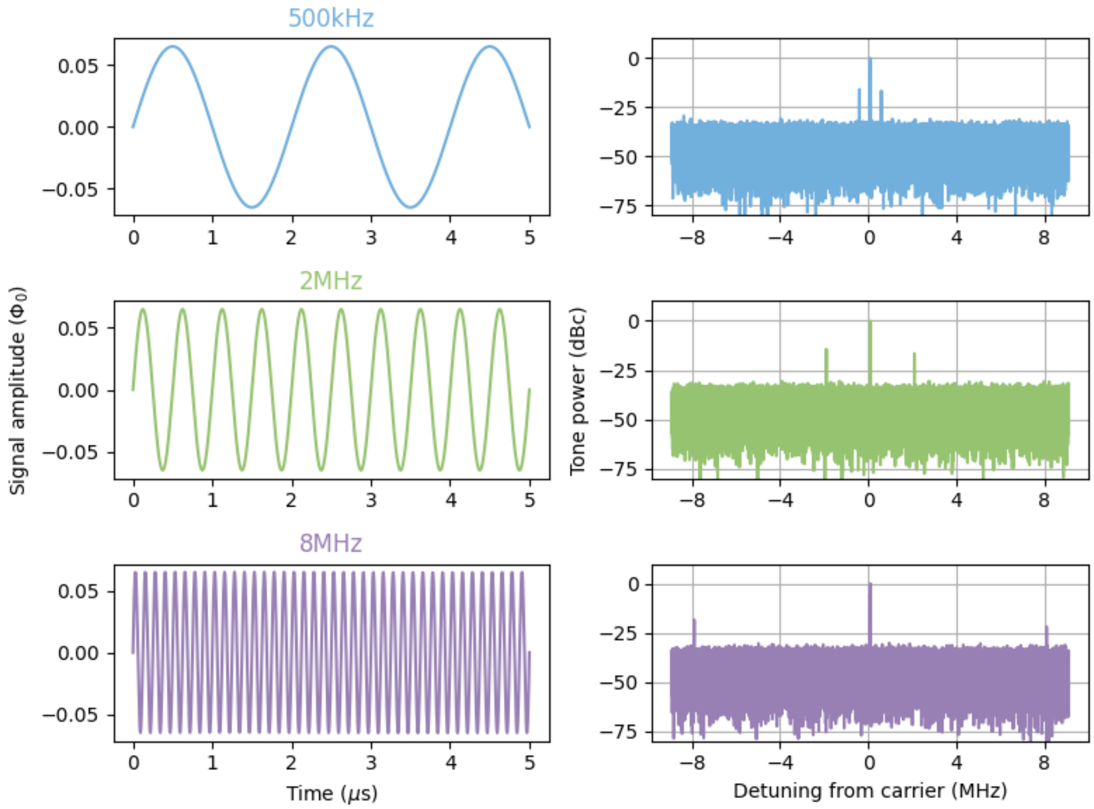

Fig 6: A demonstration of upconversion taken with our RQU. By applying a signal of 500kHz, 2MHz, and 8MHz to our input coils, we were able to see sidebands detuned from the 5.2591 GHz carrier wave by the MHz signal frequencies.

In addition, the spectrum analyzer was used to demonstrate phase-sensitive amplification in our RQU. To measure only one quadrature, our RQU was driven with a beat tone, applying microwave drives of 5.259 GHz $\pm$ 3 MHz. This creates an envelope at 3 MHz, allowing the MHz signal to be measured on average in only the quadrature in phase with this envelope. Another 3 MHz 1.6 V_{pp} tone was applied to our input coils and the phase of this wave with respect to the phase of the beat tone envelope was varied. As can be seen in figure 7, there is a significant change in the reflected tone power at the output of the RQU, with a gain extinction ratio of around 31 dB.

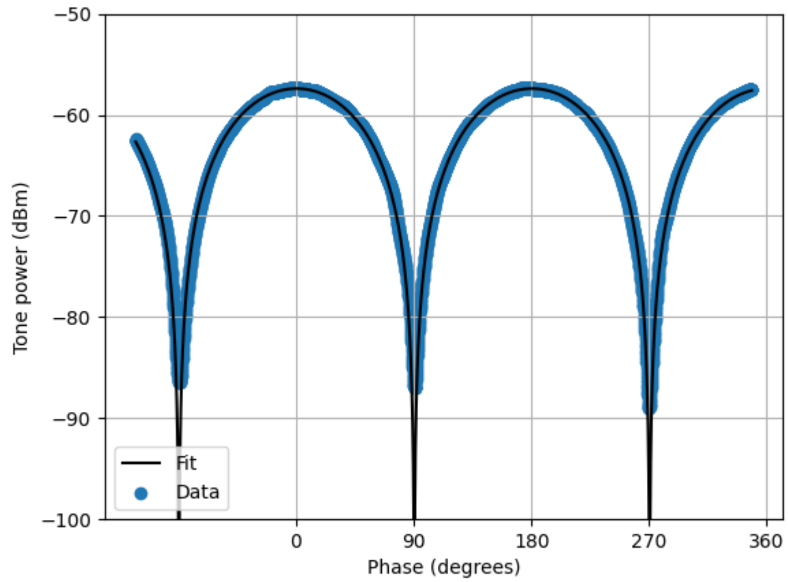

Fig 7: A demonstration of phase-sensitive amplification. For this measurement, the phase between a 3MHz envelope on a amplitude-modulated carrier wave and the 3MHz flux is varied. The tone power of the output MHz signal varies with this phase, with a gain extinction ratio of 31 dB.

5 Next Steps with RQUs

While several important measurements with the RQU have been reproduced on our new devices, the next steps are to work towards a full demonstration of backaction evasion. Currently, there are several directions to explore.

On a more immediate time scale, the current design of our RQU can be improved. Our current RQU applies a relatively small amount of flux to the interferometer - only a single Φ_0 of flux could be applied, and in doing so, our devices were heated and almost driven normal conducting. To address this, the coupling between our input coils and interferometer should be increased, which will require a redesign of our input coils and multiple added fabrication steps.

In addition, a full simulation of the RQU needs to be run to demonstrate backaction evasion. While several models of the RQU exist, these are primarily in the form of simulations on older models of RQUs, simulations calculating relevant parameters of current RQUs like geometric inductance, or theory. A full simulation of our current RQUs could guide efforts on RQU design, as well as act as a trouble-shooting tool.

On a broader scale, our goal is to demonstrate backaction evasion with our RQUs. This will require designing a high quality factor MHz resonator to couple with our GHz resonator, so spurious backaction noise can be reduced. In addition to demonstrating backaction evasion, another broad goal is to produce a protocol for measuring backaction noise.

Acknowledgments

We would like to thank the High Energy Particle Consortium for Advanced Training for funding this research. In addition, we would like to thank the members of the Irwin Group at Stanford University for their guidance and assistance in producing these results.

References

1 A. Blais, J. Gambetta, A. Wallraff, *et al.*, "Quantum-information processing with circuit quantum electrodynamics," *Phys. Rev. A* **75**, 032329 (2007).

2 S. Chaudhuri, P. W. Graham, K. Irwin, *et al.*, "Radio for hidden-photon dark matter detection," *Phys. Rev. D* **92**, 075012 (2015).

3 J. L. Ouellet, C. P. Salemi, J. W. Foster, *et al.*, "First results from abracadabra-10 cm: A search for sub-$\mu\mathrm{eV}$ axion dark matter," *Phys. Rev. Lett.* **122**, 121802 (2019).

4 A. Phipps, S. E. Kuenstner, S. Chaudhuri, *et al.*, "Exclusion limits on hidden-photon dark matter near 2 nev from a fixed-frequency superconducting lumped-element resonator," in *Microwave Cavities and Detectors for Axion Research*, G. Carosi and G. Rybka, Eds., 139–145, Springer International Publishing (2020).

5 N. Crisosto, P. Sikivie, N. S. Sullivan, *et al.*, "Admx slic: Results from a superconducting lc circuit investigating cold axions," *Phys. Rev. Lett.* **124**, 241101 (2020).

6 L. H. Nguyen, A. Lobanov, and D. Horns, "First results from the WISPDMX radio frequency cavity searches for hidden photon dark matter," *Journal of Cosmology and Astroparticle Physics* **2019**, 014–014 (2019).

7 A. Garcon, D. Aybas, J. W. Blanchard, *et al.*, "The cosmic axion spin precession experiment (CASPEr): a dark-matter search with nuclear magnetic resonance," *Quantum Science and Technology* **3**, 014008 (2017).

8 S. Chaudhuri, K. Irwin, P. W. Graham, *et al.*, "Optimal impedance matching and quantum limits of electromagnetic axion and hidden-photon dark matter searches," (2021).

9 S. Chaudhuri, K. D. Irwin, P. W. Graham, *et al.*, "Optimal electromagnetic searches for axion and hidden-photon dark matter," (2021).

10 S. E. Kuenstner, E. C. van Assendelft, S. Chaudhuri, *et al.*, "Quantum metrology of low frequency electromagnetic modes with frequency upconverters," (2022).